Supporting Information

Wu et al. 10.1073/pnas.1504920112

SI Text

S1) Derivation of the Wind-Chime Model

Each pulse generates an angular momentum on each MoS_2 flake that makes them rotate unless they develop an axis parallel to the laser beam polarization. This is also associated with rotation of a small portion of the liquid nearby the flake surface. Then, the viscous force at the flake edge reduces the angular velocity exponentially until it becomes static. When the next pulse arrives, the same process repeats, where the integrated result is the macroscopic angular motion of the flake (i.e., the formation of the wind chime).

Taking $E(z,t)=E_0e^{-((ct-z)^2/c^2\tau^2)}\sin(kz-\omega_0 t)$, where τ is pulse width, we have $I=\varepsilon\overline{E^2}c=(c/2T)\varepsilon_0E_0^2\tau\sqrt{\pi/2}$, where T is the period of pulse repetition and we have assumed $2\pi/\omega_0 << \tau$. The electrical polarization in the flake domain is $\boldsymbol{P}=(\varepsilon_r-1)\varepsilon_0\boldsymbol{E}\cos\theta$. In molybdenum disulfide the electrical field is $\boldsymbol{E}/\varepsilon_r$. Thus, assuming a circular disk shape for the flake domains, the rotation torque generated by the laser pulse $\mathcal{M}=\int|\boldsymbol{P}\times\boldsymbol{E}|\,dV$ has a magnitude of

$$\mathcal{M}=\frac{1}{4}\sin 2\theta\frac{(\varepsilon_r-1)}{\varepsilon_r}\varepsilon_0E_0^2\pi R^2he^{-\left(2(ct-z)^2/c^2\tau^2\right)}, \qquad [S1]$$

where R is the disk radius and h is the disk thickness. Thus, when a pulse traverses the disk, the initial angular velocity acquired is

$$\Omega_0=\frac{\int\mathcal{M}dt}{J_{MoS_2}+J_{Solution}}=\frac{\frac{1}{4}\sin 2\theta\frac{(\varepsilon_r-1)}{\varepsilon_r}\varepsilon_0E_0^2\pi R^2h\sqrt{(\pi/2)}\tau}{J_{MoS_2}+J_{Solution}}. \qquad [S2]$$

Considering Newton's fluid with constant viscosity coefficient η and linear velocity v at the interface between the rotating and nonrotating parts, the rotation torque $\mathcal{V}$ due to the viscous force is

$$\mathcal{V}=\eta\int_0^{\pi}\frac{dv}{dr}(R\sin\varphi)(\xi\cdot 2\pi R\sin\varphi)(Rd\varphi)=\pi\eta\Omega\xi R^3, \qquad [S3]$$

where Ω is the rotation velocity and ξ is the portion of the globe that is rotating together with the disk. Here ξ assumes a value between 0 and 1 and we estimate it to be closer to 0, because for each pulse the rotation has to be slow and not much fluid will sense the rotation before it reaches the static state. Hence in the relaxation process induced by the viscous force we obtain $\Omega=\Omega_0e^{-(\pi\eta\xi R^3/(J_{MoS_2}+J_{Solution}))t}$. With Eq. **S2**, the rotation angle accumulated due to each single light pulse is thus

$$\delta\theta=\int_0^T\Omega dt\approx\int_0^{\infty}\Omega_0e^{-\left(\pi\eta\xi R^3/\left(J_{MoS_2}+J_{Solution}\right)\right)t}dt=\frac{(\varepsilon_r-1)}{\varepsilon_r}\frac{2TIh}{4\eta\xi Rc}\sin 2\theta. \qquad [S4]$$

The time for the pattern formation is

$$\sum_{i=1}^{N}\delta\theta_i=\frac{(\varepsilon_r-1)}{\varepsilon_r}\frac{2TIh}{4\eta\xi Rc}\cdot N\cdot\overline{\sin 2\theta_i}, \qquad [S5]$$

where N is the number of laser pulses. Assume that the pattern formation time is approximately that needed for a flake at $3\pi/8$ to rotate to $\pi/8$. Thus, we have $\overline{\sin 2\theta_i}\sim 0.86$ and $\sum_{i=1}^{N}\Delta\theta_i=\pi/4$. Therefore, the time needed for the pattern formation is

$$\mathcal{T}=N\cdot T=\frac{\varepsilon_r\pi\eta\xi Rc}{1.72(\varepsilon_r-1)Ih}=0.3\text{ s}, \qquad [S6]$$

where we have used the values $\varepsilon_r=3.33$ for MoS_2, $\eta=3.2\times10^{-4}$ Pa·s for acetone, $R\sim 1$ μm, $h\sim 10$ nm, $I=250$ W/cm^2, and $\xi\sim 0.03$ in our experiment. As a result, $\mathcal{T}$ does not depend on the laser repetition rate. In the extreme condition when the rate is approaching infinity, the above derivation approximately accounts for the case of a continuous wave laser beam excitation. So we have actually considered situations of both pulsed and cw laser beam excitations and the results are identical. This has been verified in our experiment. Note that apparently T is inversely proportional to the laser intensity. However, the value of ξ is somehow positively correlated to the intensity at a certain range of I. So the actual time T is not tightly dependent on the laser intensity either, which has also been confirmed in our experiment.

S2) Comparison of $\chi^{(3)}$ with Calculated Absorption Along z

From Fig. S1 it can be seen that our experimental results do not compare well with the theoretical absorption along z. At below 2 eV, the measured values are a few times higher than that of the theoretical calculation.

S3) Ring Number of the 532-nm Pattern as a Function of the Total Laser Intensity

In the main text we discussed the ring number of the 473-nm pattern. Here we show the other aspect of the same data (Fig. 5*A*) by illustrating the ring number of the 532-nm pattern (Fig. S2).

S4) Relation Between the Fringe Thickness and the Flake Concentration

As shown in Fig. S3*A* (*Upper* panel is adopted from ref. 22 and *Lower* panel is adopted from ref. 14), the fringes are interfering results of the output beams having an identical wavevector. The width of the ring peak is determined by, for a given angle change in the wavevector, how much phase change is occurring ($k_\perp(r)=d\Delta\psi(r)/dr$). The larger $\chi^{(3)}$ is (or equivalently n_2), the more phase change, and hence the narrower the fringe. It is worth noting that both the bright and dark fringes change simultaneously. If more MoS_2 flakes are under illumination, the width becomes narrower due to enhanced $\chi^{(3)}=\chi^{(3)}_{total}$.

In Fig. S3*B* we show the results from two different samples. Fig. S3*B*, *Left* corresponds to a sample that has 85% MoS_2 concentration of that of Fig. S3*B*, *Right*; thus there are 85% MoS_2 flakes illuminated. All other factors of the experiment, including the screen and camera positions, are identical. Thus, $\chi^{(3)}_{left}=(M_{left}/M_{right})^2\chi^{(3)}_{right}$, number of rings $N_{left}=(M_{left}/M_{right})^2N_{right}$, and ring diameter $D_{left}=(M_{left}/M_{right})^2D_{right}$, where M is the effective number of MoS_2 layers [note that in *Methods* we have $\chi^{(3)}=M^2\chi^{(3)}_{onelayer}$]. In Fig. S3*B*, the ring diameter is enlarged by $(M_{right}/M_{left})^2=(1/0.85)^2=1.4\times$ and the number of rings is also enlarged by 1.4×. Therefore, the absolute ring thickness is unchanged (parallel white straight lines in Fig. S3*B*). However, the relative fringe thickness is narrowed: Because the number of rings is enlarged by 1.4×, the relative fringe thickness (absolute thickness divided by the ring diameter D) is narrowed by 1.4×, too. Conversely, if one takes the jth ring counted from the ring center, both its absolute and relative thicknesses are narrowed.

S5) Absorption and Raman Spectra of the MoS_2 Flakes

The absorbance of our MoS_2 suspension is shown in Fig. S4*A*. It is different from that in ref. 2. Rather, it can be understood based on the results in ref. 29. In ref. 29 red shift has been observed for the multilayer samples. The red shift in the absorption peak of our result demonstrates that most of the flakes in our sample are not monolayer MoS_2 flakes. Here the suspension modifies the background tendency of the absorption. We also measured the Raman scattering of the flakes from the suspension (Fig. S4*B*). Comparison with that in ref. 30 shows that our sample is composed mainly of few-layer MoS_2 flakes.

S6) Estimation of the Sample Concentration

The concentration of our MoS_2 suspension solution is ρ = 0.00085 mol/L. The volume is $V = 4 \times 10^{-3}$ L. Thus, the total number of molecules in our solution is $M = \rho \times V \times N_A = 2 \times 10^{18}$. The space group of bulk MoS_2 is $P6_3/mmc$ hexagonal and the lattice constants are a = 3.161 Å and c = 12.295 Å, respectively. Thus, a single effective layer contains $m = S$/unit cell area in ab section = 1×4 cm^2/(sin 60°) × (3.161)^2 Å^2 = 4.6×10^{15} molecules. Hence the layer number is n = M/m = 444. Due to the instability of the suspension, we estimate the effective layer number to be 300.

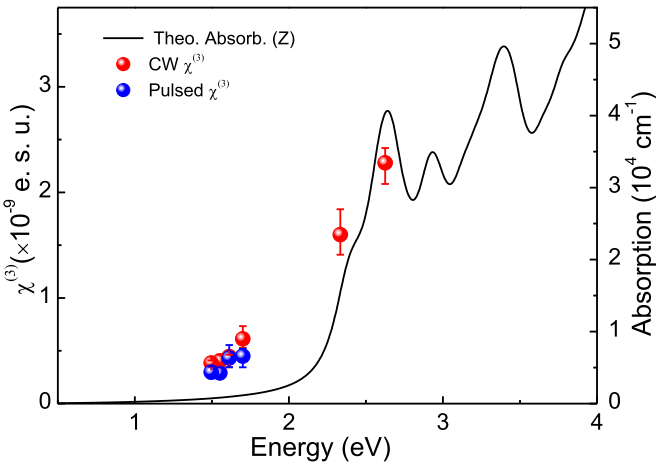

Fig. S1. Comparison of the gap-dependent $\chi^{(3)}$ with the calculated absorption. The blue and red spheres represent the pulsed and cw laser excitation results.

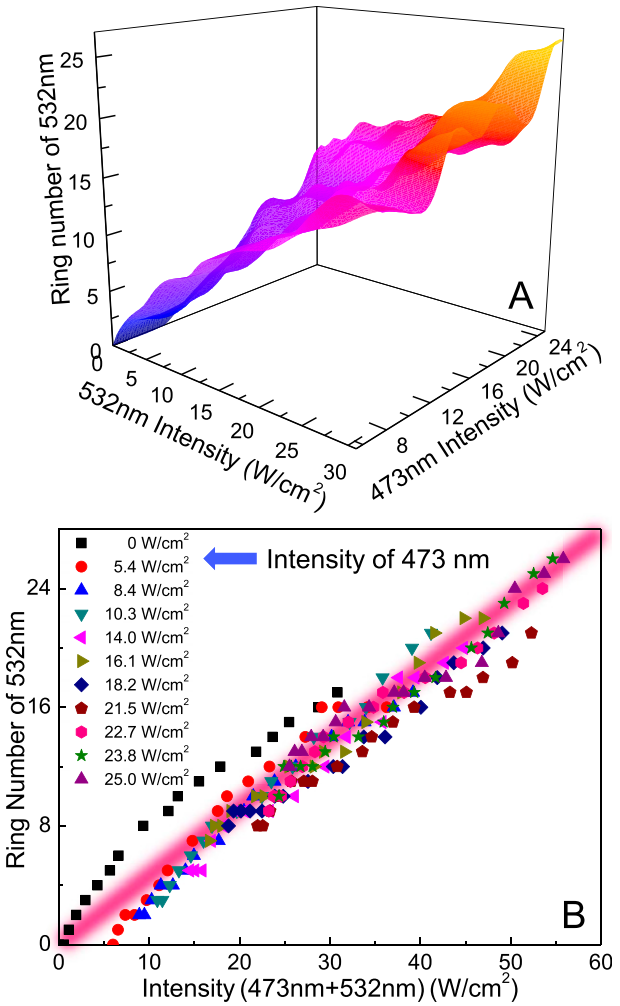

Fig. S2. Two-color all-optical switching based on SSPM. (*A* and *B*) Ring number of the 532-nm pattern, which is proportional to the sum intensity of the 532-nm and 473-nm laser beams. (*A*) Three-dimensional plotting of the results in *B*. (*B*) Data of multiple 473-nm laser fluences. The wide diagonal red line is a guide to the eye.

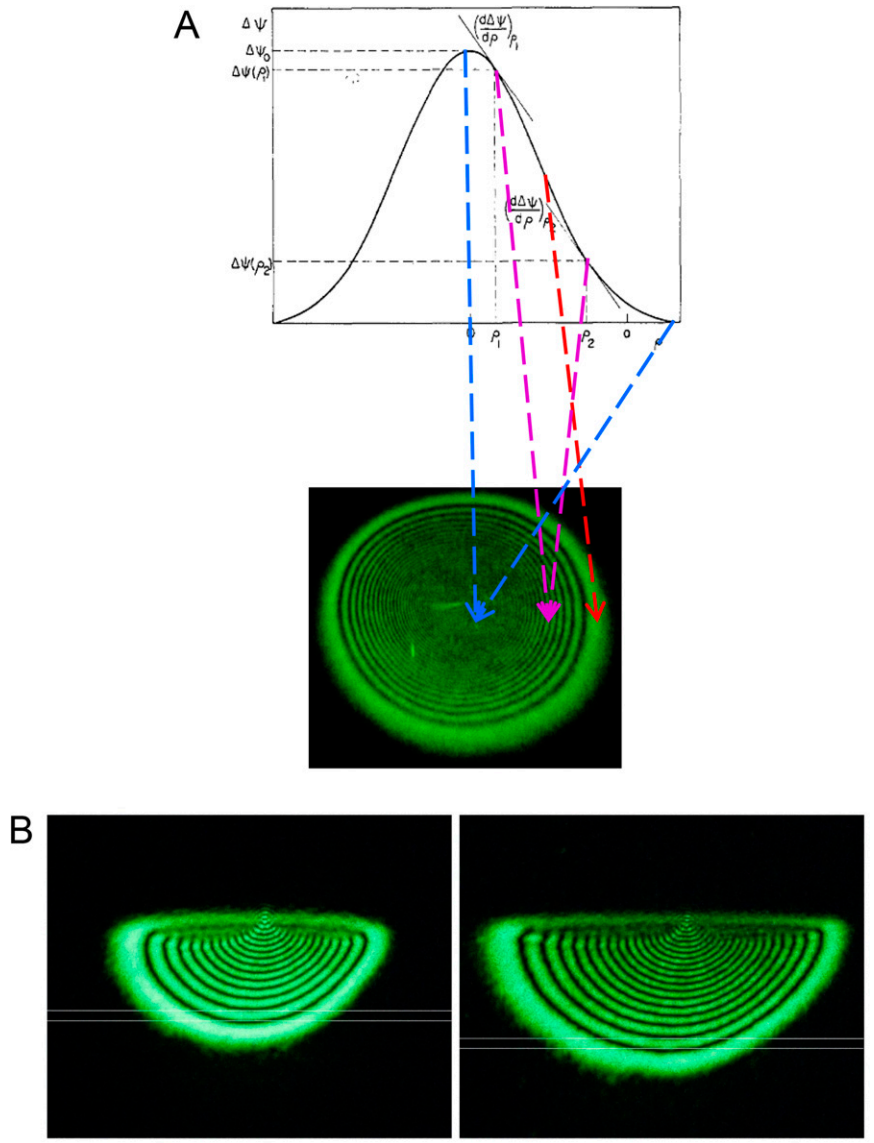

Fig. S3. Sample density dependence of the fringe thickness. (*A*) Illustration of the parallel wavevector and fringe formation. Note the difference in the fringe thickness. (*B*) The fringe thickness, depending on the solution density. *B*, *Right* corresponds to a sample with higher MoS_2 density. The white lines are used to mark the absolute fringe thickness.

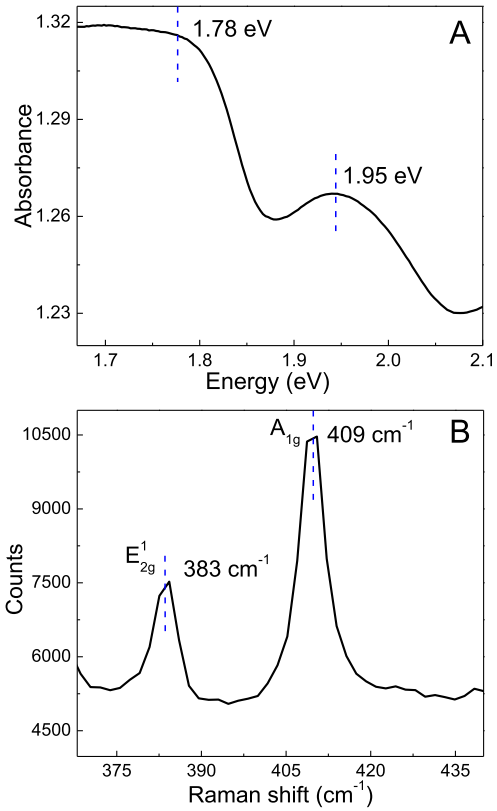

Fig. S4. Sample characterization. (*A*) Absorption spectra of the MoS_2 flake suspension. (*B*) Raman shift of the MoS_2 flakes after the evaporation of the solution.